This is the Accepted Manuscript version of a Published Work that appeared in final form in Energy Conversion and Management 224 : (2020), 113327. To access the final edited and published work see https://doi.org/10.1016/j.enconman.2020.113327
© 2020 This manuscript version is made available under the CC-BY-NC-ND 4.0 license https://creativecommons.org/licenses/by-nc-nd/4.0/

Lessening coke formation and boosting gasoline yield by co-cracking scrap tire pyrolysis oil in the conditions of an FCC unit

Elena Rodríguez[a], Sepideh Izaddoust[a], José Valecillos[a], Javier Bilbao[a], José M. Arandes[a], Pedro Castaño[a,b], Eva Epelde[a], Gorka Elordi[a]*

a. Chemical Engineering Department, University of the Basque Country UPV/EHU, P.O. Box 644-48080, Bilbao, Spain

b. Multiscale Reaction Engineering, KAUST Catalysis Center (KCC), King Abdullah University of Science and Technology (KAUST), Thuwal 23955-6900, Saudi Arabia

Abstract

We have studied the effect of adding scrap tire pyrolysis oil (STPO) as feed or co-feed in the cracking of vacuum gasoil (VGO) using a commercial equilibrated catalyst. The cracking experiments were performed in a laboratory scale fluid catalytic cracking (FCC) simulator using VGO, STPO, or a blend of the two (20 wt% of STPO), contact time = 6 s, catalyst/feed ratio = 5, and 530 ºC. The composition of the different feeds has been correlated with the yield of products and the amount-location-nature of the deactivating species (coke). Our results indicate that the addition of STPO has very positive outcomes in terms of higher gasoline yield of enhanced quality and composition, while quenching deactivation. STPO yields less amounts of coke, which is more aliphatic, lighter, and located in the micropores of the catalyst. The complete analysis of the coke fractions (soluble and insoluble) have lighted the peculiar chemistry of these species as a function of the type of feed used. The results point to a viable and economically attractive valorization route for discarded tires.

Keywords: tire recycling; waste valorization; fluid catalytic cracking FCC; deactivation; coke

Introduction

End of life tire (ELT) management is becoming one of the most important environmental issues worldwide. Almost 1.3-1.5 billion tires are produced every year, giving way to approximately 17 Mt of used tires [1,2]. According to the European Tyre & Rubber Manufacturers' Association (ETRMA) [3], around 95% of ELTs (accounting for more or less 2 million metric tons of scrap tires) are recycled or recovered for material (40%), energy (38%), reconstruction (7%), and reuse/export (10%) purposes [4–6]. However, in many countries the remaining waste tires are still dumped, although its disposal in landfills is being banned (i.e. EU) [7], as it contributes to serious environmental and human health problems (e.g. risk of spontaneous fires or diseases caused by mosquitoes and rodents) [1]. The environmental impact derived from chemical leaching, waste tire combustion and incineration, particulate pollution, as well as the presence of micro-plastics (MPs) in the oceans is also attracting great concern [8–10].

In this sense, several alternative valorization routes, i.e. gasification [11–15] and pyrolysis [7,16–19] are emerging. Particularly, the flash pyrolysis of waste tires gives way to three main product fractions, which are highly dependent on the type of tires, the operating conditions, and the reaction technology used [1,20–22]: a gas phase, with a high energy content; a solid product (adulterated carbon black), to be valorized via gasification or applied as adsorbent or catalyst support (after sulfur removal); and, a liquid phase, so-called scrap tire pyrolysis oil (STPO), with promising prospects for fuel blending [6,7,23,24] and for the production of added-value chemicals, such as aromatics BTX (benzene, toluene and xylenes) [25–27] and limonene [28], among others. However, the STPO shows several drawbacks for being directly used as automotive fuel, due to its high content in heteroatoms and aromatics. Furthermore, several pretreatments are needed to comply with emission legislations [29]. In this context, the use of

available and amortized refinery units (mainly fluid catalytic cracking, FCC, and hydroprocessing units) could contribute to intensify high-quality fuel production from these non-biodegradable wastes (Waste Refinery) [5,30]. FCC units and catalysts have shown an outstanding versatility to treat non-alternative feedstock, usually blended with vacuum gas oil (VGO) [31,32], such as, secondary refinery streams (naphtha, waxes, resids) [33–37], biomass-derived feeds (bio-oil, pyrolysis oil, vegetable oils and animal fats) [38–47], and plastic wastes [48,49]. The possibility of upgrading STPO alone and/or blended with VGO has been reported by several authors [29,50,51].

A conventional FCC unit is provided with a fluidized bed reactor, with vertical transportation of both the catalyst and feed/products (riser), a stripper, and a fluidized bed regenerator [36]. FCC catalysts have greatly evolved over the years, from natural clays and silica and alumina catalysts to zeolite Y based catalysts. The main challenges for catalyst design are aimed to improve [37]: (i) activity, selectivity, and accessibility; (ii) resistance to attrition; (iii) hydrothermal stability; (iv) metal tolerance, in the case of feeding heavier feedstocks; (v) hydrodynamics related to fluidization; and (v) catalyst stability, by minimizing coke selectivity. A typical FCC catalyst is composed of a stabilized form of zeolite Y as an active phase, clay as filler, and alumina and/or silica sources to provide a meso- and macroporous matrix. The components are usually mixed in an aqueous slurry, and then spray-dried to obtain almost uniform spherical particles to facilitate the fluidization in the regenerator. Several initiatives to enhance zeolite Y catalytic performance include adding rare earth metals and providing hierarchical porous structure, among others [31,37,52].

Together with the catalyst properties, the operating conditions and feed composition also have a great influence on product distribution and coke deactivation, due to the complex reaction

network, where several acid catalyzed reactions are involved [31,37,52]: β-scission, protolytic cracking, isomerization, hydrogen transfer, cyclization, and aromatization. Coke formation also has a crucial impact on catalyst performance and product distribution, as well as in the heat balance of the FCC unit [53,54]. It can be formed from the condensation and dehydrogenation of hydrocarbons (catalytic coke), but also from thermal cracking (thermal coke), from heavy molecules present in the feed (Conradson coke), dehydrogenation reactions catalyzed by metal poisoning or from entrained catalytic products in the small pores, not having been removed by stripping [31,54]. Hence, coke deactivation entails active site deactivation, thermal aging and pore blockage, among others. Successive reaction-regeneration cycles can also damage the crystalline structure of the catalyst and affect the morphology of the coke [55].

Special efforts are made in the recent literature to contribute to a better understanding of the deactivation phenomena on FCC catalysts. Cerqueira et al. [54] and more recently, Bai et al. [31] have reviewed the latest findings on this issue, by focusing on: (i) the origin of coke and its location on the catalyst surface [56]; (ii) multi-technique catalyst characterization [57]; (iii) deactivation mechanisms for different contaminants; as well as, (iv) technical approaches to controlling coke deactivation. Moreover, recent studies on the deactivation of FCC catalysts at the single particle level are positively contributing to this field as well [58–62].

In this work, we have studied the possibility of upgrading STPO as feed or co-feed together with VGO in an FCC unit. We have analyzed the synergetic effects of both feeds on product distribution (mainly gasoline), and, especially on coke deactivation. For this purpose, based on the extensive previous work of Rodriguez et al. [29,30,51] we have selected a temperature of 530 ºC, where the effect of deactivation is significant, and a blend of 20 wt% of STPO and 80 wt% of VGO, as the most suitable co-feeding ratio, allowing to treat the STPO derived from the tires

collected in a large geographic area. This study contributes to a better understanding of coke deactivation from non-conventional feedstock to be treated in FCC units in order to approach the future waste-refinery concept, where wastes of consumer society will be valorized, such as plastics and tires, among others. In order to correlate the coke features (coke content, nature, and its location) with those of the feeds, we have developed an exhaustive coke characterization study by the following techniques: N_2 adsorption-desorption; temperature programmed oxidation (TPO); Fourier transform infrared (FTIR) spectroscopy; TPO-MS (mass spectrometry) coupled with FTIR spectroscopy; Raman spectroscopy, laser desorption ionization time-of-flight mass spectroscopy (LDI TOF-MS), and soluble coke characterization by GC-MS.

2. Experimental

2.1. Feeds

The vacuum gas oil (VGO) as the standard feed of the FCC unit was provided by Petronor S.A (Muskiz, Spain) and scrap tire pyrolysis oil (STOP) was produced by flash pyrolysis of waste tires in a conical spouted bed reactor at 500 ºC. The reaction system and operating conditions were described in previous works in detail [63,64]. A blend of STPO (20 vol%) in VGO was provided to evaluate the synergy effect of co-feeding on the cracking of VGO. To determine the composition of the feeds, simulated distillation analyses were performed in an Agilent 6890 Series GC gas chromatograph, based on the ASTM D-2887 standard. The complementary information of feeds' composition was provided by means of a two-dimensional Agilent 8790A series gas chromatograph (GC×GC) coupled with an Agilent 5975C Series mass spectrometer (MS). The device is equipped with two non-polar and polar capillary columns, a flow modulator, and mass spectrometer (MSD) and flame ionization detectors (FID) [5]. Elemental analysis of

both feeds was carried out with a TruSpec CHN Macro LECO device, using an additional TruSpec S module for the S [51].

Density of VGO and STPO were calculated according to ASTM D4052. Their API was estimated by means of the 2B2.3 procedure of the API technical data book based on ASTM D287. Viscosity of both feeds was determined following the procedure 11A4.2 of the technical data book of API. The average molecular weight of the feeds was calculated from the kinematic viscosity following procedure 2B2.3 of the API technical data book. The high heating value (HHV) was determined by differential scanning calorimetry (DSC), with a Setaram TG-DSC 111 calorimeter coupled with thermogravimetric analysis equipment. The experimental procedure consists of the combustion of the feed with air following a 5 ºC min^{-1} temperature ramp from 20 to 750 ºC and holding it for 20 minutes before cooling it down to the initial temperature [52].

2.2. Fresh and coked catalyst characterization

An equilibrium commercial FCC catalyst containing 15.5% zeolite HY and supplied by Petronor refinery (formerly used in the refinery) was utilized in this work. To determine the textural properties of the catalyst, N_2 adsorption-desorption analysis was carried out in a Micrometrics ASAP 2010 device, which included two steps of sample degasification at 150 ºC under vacuum for 8 h followed by introduction of N_2 in multiple equilibrium stages at 77 K to saturate the sample. Specific surface area, pore volume and pore distribution, and material content of zeolite were determined by BET, BJH, and Johnson methods, respectively [52].

X-Ray-diffraction patterns of catalyst crystal structure were obtained on a Philips PW 1710 diffractometer, where the tube anode was Cu with $K\alpha = 1.54242$ Å and operated at 40 kV and 40 mA in theta-theta configuration. An energy dispersive PIXcel detector was used with an active length of 2q = 3.347 Å. To obtain the unit cell size, the ASTM D3942-85 standard was followed

by the signals' intensity measured at reflection angles correlated to spent zeolites (Al: 23.5º, 26.9º and 31.2º; Si: 28.5º). Component analysis of the catalyst was performed in Thermo Fisher scientific XSeries II quadrupole ICP-MS equipped with an Xt interface and concentric nebulizer.

In order to measure the catalyst's total acidity and distribution of acidic strength by temperature-programmed desorption (TPD) of NH_3 (adsorbed at 150 ºC) a TG-DSC Setaram 111 calorimeter connected to a mass spectrometer (Blazers Instrument Thermostar) was used [65]. To determine the nature of acid sites (Brönsted/ Lewis (B/L) acid site ratio), a high pressure high temperature Specac cell connected on-line with a Nicolet 6700 FTIR spectrometer was used to record the spectra of adsorbed pyridine at 100 ºC, analyzing the bands at 1545 (Brönsted acid sites) and 1450 cm^{-1} (Lewis acid sites) [52]. The acidity and physical properties of the commercial catalyst are shown in Table 1.

Table 1. Acidity data and physical properties of the commercial catalyst used.

Zeolite content (wt%)	13.8
Unit cell size (Å)	24.26
Bed density (g cm^{-3})	0.90
Particle size distribution:	
< 40 µm (wt%)	0
< 80 µm (wt%)	67
< 105 µm (wt%)	87
< 149 µm (wt%)	99

Fig. 1 summarizes the different techniques used for the characterization of the coked catalyst samples. The deterioration of physical properties of the coked catalyst samples as well as coke location were analyzed by N_2 adsorption-desorption using the same method applied for fresh catalyst. The coke content of the samples was estimated by temperature programmed oxidation (TPO), using a TA Instruments TGA-Q 5000 thermobalance, coupled with a Balzers Instruments Thermostar mass spectrometer to measure the CO_2 generated during the combustion of the coked

catalyst with air up to 550 ºC. Prior to the combustion step, the samples were swept with a stream of N_2 at 550 °C (3 h) in order to eliminate the possible impurities.

FTIR analysis of the coked catalyst samples were performed in a Nicolet 6700 spectrophotometer (Thermo-Fisher Scientific) where samples (3-5 mg of coked catalyst mixed in 300 mg of KBr) were subjected to vacuuming at 100 ºC for 1 h. To identify the nature of coke species by the aid of combustion gases, the FTIR cell connected to a OmniStar ThermoStar GDS 320 Pfeiffer Vacuum mass spectrometer was used. The samples were primarily vacuumed at 100 ºC and consecutively exposed to temperature increases of up to 550 ºC (5 °C min^{-1}) in the presence of air (60 mL min^{-1}). The spectra were collected with scan number, 60; resolution, 4 cm^{-1} and frequency, 12 h^{-1}; concurrently CO_2 signals were recorded in the mass spectrometer. In order to determine the structure of deactivating species, Raman analysis of the coked catalysts were carried out in a Renishaw confocal microscope using two beams at the wavelengths of 514 and 785 nm, where the florescence beam originated from coke species was subtracted. Identification of polycyclic aromatic components, such as coke, was carried out by the aid of the matrix-assisted laser desorption/ionization time of flight mass spectrometry (MALDI-TOF MS) analysis technique. Due to matrix presence, the molecules' fragmentation is minimized. Therefore, the obtained mass spectrum directly points to the molecular weight of individual species as well as the molecular weight distribution of the analyzed mixture [66]. The analysis process was performed in a Nd-YAG laser-based Bruker Autoflex Speed unit (Bruker, Germany), where the sample was exposed to short pulses under high vacuum.

The coke extraction was performed by using dichloromethane (Panreac, 98% purity) as an extraction solvent, where the process included bringing CH_2Cl_2 into contact with 100-400 mg of coked catalyst in a Soxhlet extractor to obtain the coke species distributed over the zeolite and its

outer surface (external soluble coke). The procedure was followed by the addition of HF, which destroys the zeolite crystal structure and allows for the extraction of the remaining coke located inside the zeolite's micropores (internal soluble coke). Subsequently, the samples were immersed into dichloromethane to recover the remaining soluble coke that was sterically blocked inside of the zeolite micropores. Soluble coke analysis was performed on a gas chromatograph coupled with a Shimadzu QP2010 mass spectrometer (GC-MS), equipped with a 50 m × 0.22 mm × 0.25 µm BPX5 column. The structure of the insoluble coke was determined by LDI-MS, as previously described.

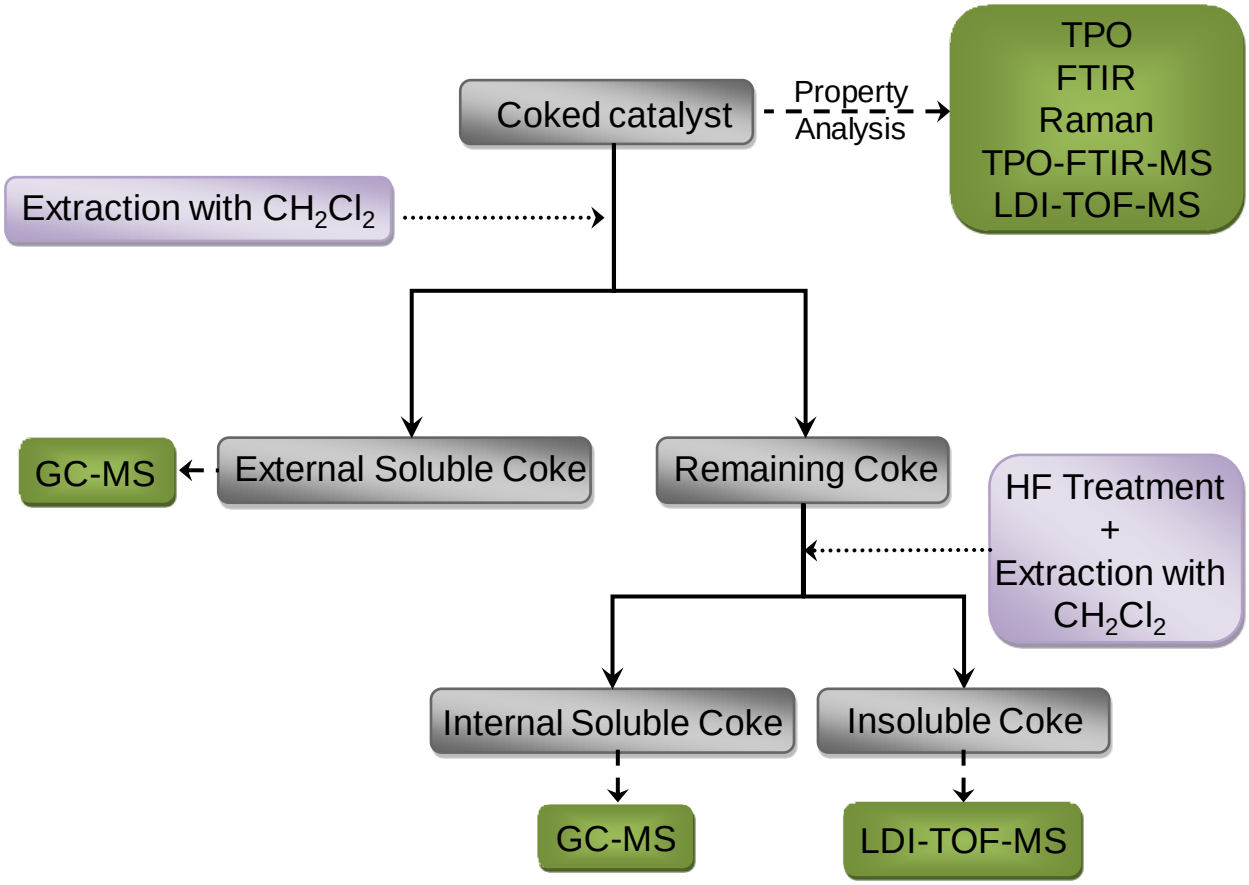

Fig. 1. Scheme of the followed steps for the characterization of the coked catalyst and the coke deposited on it.

2.3. Reaction equipment

The reaction apparatus is a CREC riser simulator, where the predetermined amount of fluid reactants undergoes cracking in gaseous phase. The reactor consists of a confined volume (basket) restricted to two grids placed on the top and lower sides of the basket to retain the catalyst fluidization inside of the chamber, whereas its porous conformation facilitates feed circulation through the basket volume. To mimic industrial conditions, an impeller has been located on top of the basket to provide a continuous fluidization of feed between the up-flow and down-flow zones, as well as its uniform concentration inside of the chamber. Gaseous reactants are introduced at the predefined temperature into the reactor. Once the reaction occurs and the preset residence time elapses, the reactor and vacuum box (320 ºC) are connected and the reaction mixture is withdrawn from the reactor basket towards the vacuum box by the aid of the vacuum state previously imposed on the system. Experiments were carried out under the following operating conditions: reaction temperature, 530 °C; residence time, 6 s; catalyst/feed mass ratio, 5 $g_{catalyst}(g_{feed})^{-1}$. Product streams were consequently sent to the gas chromatograph to be analyzed.

2.4. Products analysis

Product analysis was carried out in a gas chromatograph (Agilent Technologies 7890), equipped with an HP-PONA Column (Agilent Technologies, 50 m long, 0.2 mm internal diameter and 0.5 μm in thickness and capable of operating from -60 up to 325 ºC and using He as the carrier gas) and two FID and PFPD (embedded to detect sulfur components) detectors. Once the reaction mixture (including product and feed) is collected in the loop, the turning of the six-port valve allows He to drag the gases from the loop towards the gas chromatograph through the thermostated line (320 ºC). The analysis starts at -30 ºC (3 min) to ensure the detection of the

most volatile compounds, followed by two linear temperature programs: first, an increase to 235 ºC with a ramp of 15 ºC min^{-1}, keeping it constant for 1 minute to elute most of the products; next, the temperature is increased (30 ºC min^{-1}) to 320 ºC to elute the heaviest components and uncracked feed. Identification of the products was carried out by means of a gas chromatograph coupled with a mass spectrometer (GC-MS), model QP2010 of Shimadzu, equipped with a BPX5 column of 50 m × 0.22 mm × 0.25 μm, Y and NIST library.The sulfur content of cracking products has been determined with the PFPD detector previously calibrated with sulfur compound standards [5].

3. Results

Properties of the catalyst used were previously mentioned in Table 1 of the experimental section. These features correspond to a typical equilibrated FCC catalyst. The elemental analysis and the physical properties of the used feeds are shown in Table 2. As can be seen, the VGO is a slightly more hydrogenated sample, whereas STPO contains larger amounts of nitrogen, albeit nearly equal amounts of sulfur. Regardless, STPO has a more volatile nature, as proved in the simulation distillation curves of Fig. 2. Due to the latter, it has lower density, a higher value of API gravity, less viscosity, and lower average molecular weight (M_w) than VGO. On the other hand, the high heating values (HHV) of both feeds are relatively similar.

The GC×GC analysis of VGO indicates that a fraction of 62.3 wt% is aromatics, followed by 29.2 wt% naphthenes, 8.5 wt% paraffins, and 5.5 wt% sulfur-containing compounds. On the other hand, the composition analysis of STPO reveals 55.8 wt% aromatics, 34.4 wt% naphthenes, 7.1 wt% olefins, 2.4 wt% paraffin, and 11.6 wt% sulfur-containing compounds [29]. Simulated distillation results (Fig. 2) reveals that VGO is made up of 95.5 wt% heavy compounds (with their boiling point above that of diesel) and contains 1.5 and 3 wt% distillates

in the gasoline and diesel fractions, respectively. The STPO is constituted by more volatile compounds as compared to the VGO, with 15.5 wt% in the range of the gasoline fraction, 29.3 wt% in the diesel fraction, and 55.2 wt% in the fraction heavier than diesel. Based on these data, the STPO+VGO mixture (20, 80 wt%, respectively) would contain 4.3, 8.3, and 87.4% of compounds in the gasoline, LCO, and HCO fractions, respectively. Therefore, the concentration of the gasoline fraction would be 2.8 wt% higher in the mixture than in the VGO alone.

Table 2. Elemental analysis and physical properties of the feeds used.

	VGO	STPO
Elemental analysis		
C (wt%)	86.60	87.20
H (wt%)	12.00	10.60
N (wt%)	0.23	1.04
S (wt%)	1.17	1.16
Density at 15ºC (kg L^{-1})	0.93	0.89
API gravity (ºAPI)	21.1	26.8
Viscosity at 100 ºC (cSt)	8.6	2.0
M_w (g mol^{-1})	405.3	255.8
HHV (MJ kg^{-1})	42	44

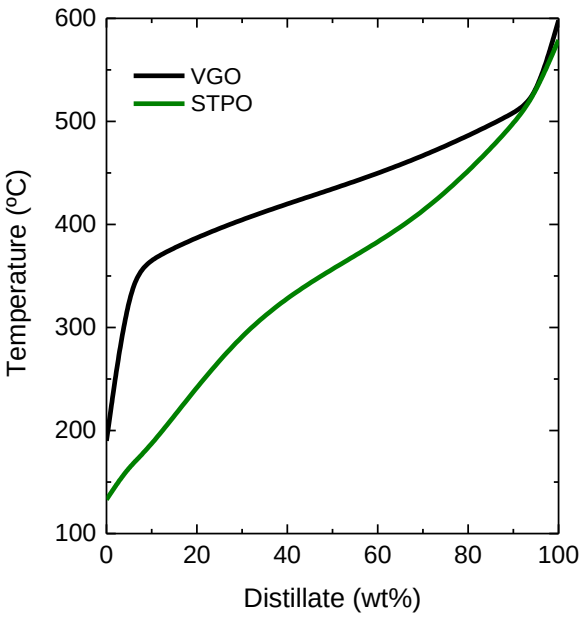

Fig. 2. Simulated distillation results for VGO and STPO.

The products of the reaction were lumped in the typical ones used in the FCC process: dry gases, C_1-C_2; liquefied petroleum gases (LPG), C_3-C_4; gasoline, C_5-C_{12}; light cycle oil (LCO), C_{13}-C_{20}, heavy cycle oil (HCO), C_{20+}, and coke. Coke was deposited on the catalyst and quantified separately by means of TPO. Fig. 3a depicts the product yield distribution of those lumps resulted from the cracking of the three feeds described under the same reaction conditions. The yield of dry gases is relatively similar, whereas the yields of LPG, HCO, and coke decrease when the amount of STPO increases in the feed. On the contrary, gasoline yield peaks for STPO and the yield of LCO is greater with the blend of the two. These results point to the adequacy of the STPO as co-feedstock in the FCC, in order to use more refractory VGO and for coping deactivation while boosting the yield of the most interesting products, in accordance with previous results [67]. The yield of coke is certainly smaller with STPO, which could be directly linked to its higher API gravity (Table 2).

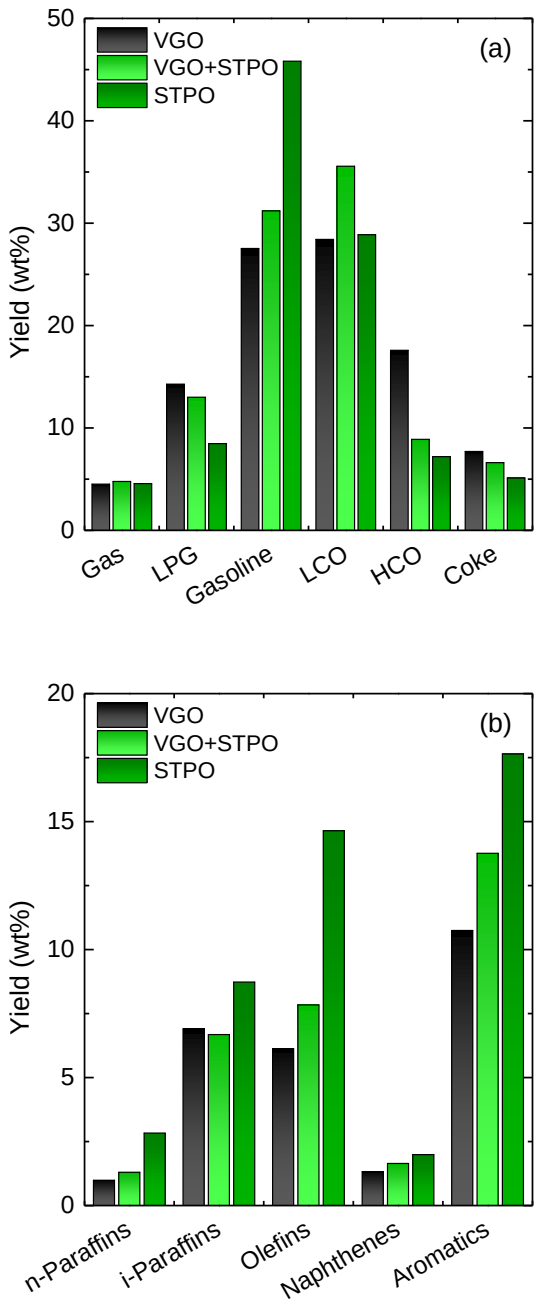

Fig. 3. Fraction yields within the products (a) and molecular families within the gasoline fraction (b) for the different feeds used.

The composition of the gasoline fraction (averaged over the entire product distribution) is shown in Fig. 3b, lumped into paraffins (linear and branched), olefins, naphthenes, and aromatics. Interestingly, regarding the gasoline fraction, increasing amounts of STPO in the feed give way to an increase in the yields of paraffins (both n- and iso-) and naphthenes, but in particular those of olefins and aromatics. This means that the addition of STPO together with the VGO or alone has a greater impact on enhancing the amount and RON index of the gasoline produced.

Physical properties of the fresh and coked catalyst samples used in the cracking of the different feeds were obtained from N_2 absorption-desorption experiments. All samples underwent a noteworthy deterioration of their physical properties associated with the activity of the catalyst. Hence, Fig. 4 depicts the extent of this degradation upon the use of the different feeds, together with the features of the fresh catalyst. The BET, micropore, and mesopore areas decrease more significantly with the use of STPO than with VGO, which means that as STPO molecules are less bulky, they diffuse better into the zeolite crystals of the catalyst, reaching the acid sites and subsequently undergoing reactions that yield more gasoline (Fig. 3a), and at the same time leaving coke deposits inside the micro- and mesopores more effectively than the VGO molecules. As a result of the loss of the micro- and mesopores, the average pore diameter (d_P) increases as the proportion of STPO in the feed increases. This effect is a result of the most effective blockage of the smallest pores (micro- and mesopores), leading to an apparent pore widening, and has been reproduced before for the cracking of other feeds [52].

The results presented so far illustrate that the presence of STPO in the feed changes the product distribution and degradation process of the catalyst. In particular, the amount of coke seems to drop (Fig. 3a) by using STPO, but the degradation of the catalyst caused by this lower amount of

coke is more severe (Fig. 4). Thus, it is of interest to further investigate the effect of STPO on the properties of coke.

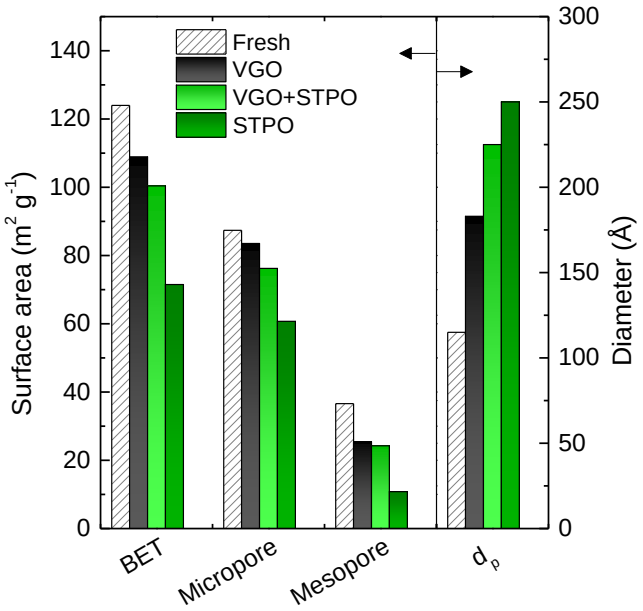

Fig. 4. Physical properties: BET surface area, mesopore area, micropore area, and mean pore diameter of the used catalyst for the different feeds used.

Fig. 5 shows the combustion profiles (TPO) of the coke samples deposited on the catalyst when treating STPO, VGO, and the blend of the two. The area under the curves represents the total amount of coke that, effectively, decreases when increasing amounts of STPO are fed. The nature of the coke seems quite similar among the samples analyzed because a unique peak is observed for the three coke samples at temperatures that do not vary significantly. The position of each combustion peak moves slightly toward lower temperatures as the feed is composed of larger molecules and the amount of coke increases: STPO; 525 ºC; STPO+VGO; 515 ºC; VGO; 505 ºC. All these values are about 50 ºC higher than those reported by Cerqueira et al. [57], which is indicative of the more refractory nature of the coke studied here, assuming that the rest

of the catalyst properties remain the same. The results indicate that the coke deposited during the cracking of STPO is more aromatic and/or located in the micropores of the catalyst. The results of Fig. 4, pointing to the higher deterioration of micropore volume for STPO, indicate that the second statement is true, whereas for the first one to be true, additional analyses are required.

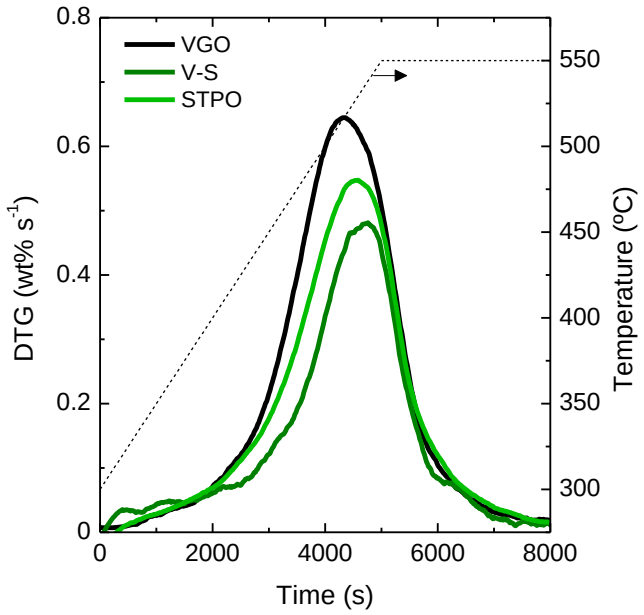

Fig. 5. TG-TPO profiles of the coked catalyst for the different feeds used.

In order to better evaluate the nature of the coke deposited on the catalyst related to the different feeds, different techniques were used, summarized in Fig. 1. The first one is FTIR spectroscopy, the spectra of which were deconvoluted according to the following bands [68–70] in Fig. 6: (a) 1580 cm^{-1}, C=C stretching bonds of aromatics, related to the presence of condensed aromatics in coke, also known as “aromatic coke band”; 1610 cm^{-1}, diolefins and conjugated double bonds, also known as “olefinic coke band”; 2922 cm^{-1}, C-H stretching bonds of intermediate and chain aliphatic groups; and 2960 cm^{-1}, C-H stretching bonds of terminal aliphatic groups. The relative intensities of these bands are fairly similar, but certain variations are due to the nature of the

feed: coke deposited on the catalyst during the cracking of VGO is more aromatic and less olefinic and aliphatic. We could anticipate this observation based on the compositions of the feed (Table 2 and Fig. 2). Besides, the TPO profiles shown in Fig. 5 correlate better with the different location of coke (Fig. 4) than its nature (Fig. 6), as was the case for the cracking of VGO and HDPE [52].

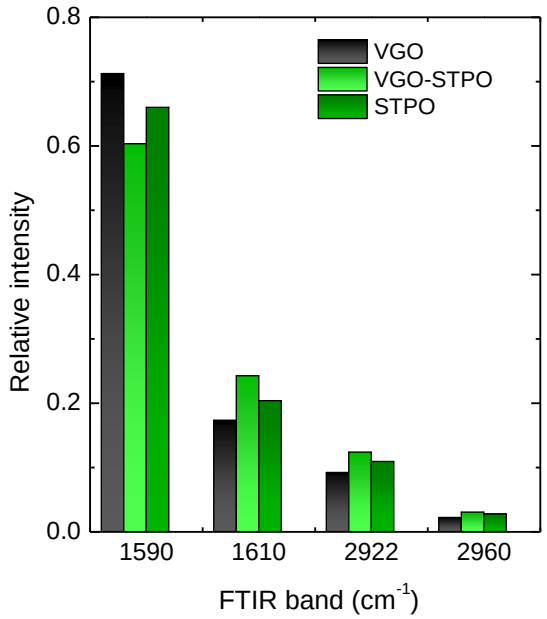

Fig. 6. Relative intensities of four bands detected in the FTIR spectra of the coked catalyst for the different feeds used.

The FTIR/MS-TPO was performed to better correlate the combustion profiles shown in the TPO (Fig. 5) with those of the FTIR bands (Fig. 6). Moreover, Fig. 7 shows these TPO profiles in terms of the CO_2 variation (m/z = 44) in the coke combustion of the coked catalysts. The intensities of four characteristic FTIR bands of coke (1590, 1622, 2922, and 2960 cm^{-1}) are shown in Figs. 7b-e for the different feeds used. The presence of two peaks compared to the TGA-TPO in Fig. 7a is due to the lack of former sweeping in the MS-TPO results. Thus, the first

combustion peak at T < 400 ºC corresponds to the combustion of the species retained in the catalyst, but not causing effective deactivation. These species desorb or "age" during the TPD sweeping performed prior to the TGA-TPO runs [71,72]. This aging can be observed during the FTIR/MS-TPO, as C=C bonds that correspond to the aromatics (Fig. 7b) and conjugated double bonds (Fig. 7c) increase, while those of aliphatics (C–H bonds of –CH, $–CH_2$, and $–CH_3$ at 2855-2955 cm^{-1}) decrease (Figs. 7d and 7e) as they are transformed into a more condensed coke. The second combustion peak at T ≈ 520 ºC corresponds to the combustion of dienes and aromatics, which are similar (in relation to their amount) to all three catalyst samples used, as seen in Figs. 7b and 7c. Interestingly, the combustion and transformation of the FTIR band at 2922 cm^{-1} is significantly higher for the coke deposited under STPO as feed, indicating the longer chain aliphatic nature of this type of coke.

The trend of selective combustion and structural evolution of coke is observed in the coke formed in the cracking of the three feeds studied, but it is more pronounced in that of STPO, because it is originally a more hydrogenated coke. It should be noted that in this coke, the disappearance of the aliphatics and the formation of polycyclic aromatics is very fast at low temperatures, revealing a rapid condensation of the coke, which could justify the peak overlap observed in the CO_2 signal of the TPO (Fig. 7a). In STPO, the high concentration of light aromatics and olefins makes it possible to attribute the role of coke precursors to these compounds, given their capacity to generate polycyclic aromatics and cyclic structures, the combustion of which is difficult to identify in the TPO analysis (Fig. 5). On the other hand, in the combustion of developed coke, the maximum of the peak is at the same temperature indicated in the TPO analysis, with the highest value (525 ºC) for the coke deposited during the cracking of STPO.

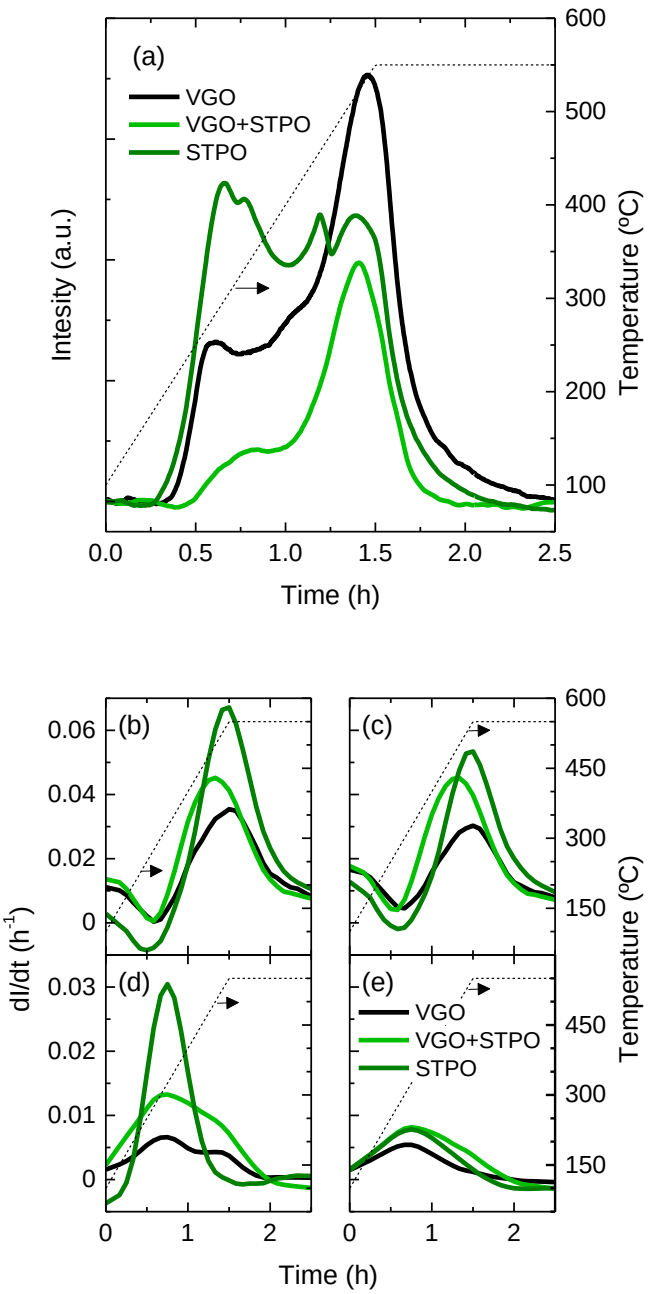

Fig. 7. TPO profiles (a) and simultaneous profiles of the FTIR intensities of the bands at 1590 cm^{-1} (b) 1622 cm^{-1} (c) 2922 cm^{-1} (d) and 2960 cm^{-1} (e) corresponding to the coked catalyst for the different feeds used.

The Raman spectra of the coked catalyst give insight into nature of the structure of the coke deposits. Fig. 8 shows the main features of these spectra deconvoluted in the following bands [68,73,74]: 1225 cm^{-1}, C–H bonds (ν_{C-H}); 1380 cm^{-1}, named D band, associated with aromatics poorly ordered or less graphitized; 1501 cm^{-1}, named D_3 band, associated with the structural defect of aromatics of poor order; 1596 cm^{-1}, named G band, condensed aromatic structures or conjugated double bonds in graphene planes and ordered networks; and 1617 cm^{-1}, named D_3 band, associated with defects in light structures of aromatics. It is worth mentioning that the deconvolution was performed assuming that the position of G band should be < 1605 cm^{-1} [75]. The results of the deconvolution of the spectra, together with the intensity relationship between the D and G bands (I_D/I_G), which is related to the size of the coke particles, are summarized in Table 3. The indices in Table 3 correspond to a developed coke, with a notable presence of aromatics, which have a remarkable level of ordering, due to the severity of the reaction conditions (high temperature and high concentration of aromatics in the feeds). However, there are notable differences for the three feeds. Thus, the coke deposited during the cracking of VGO shows a higher intensity of the D bands, which indicates a greater presence of poorly structured aromatic structures. On the other hand, the intensity of the G band is also higher, so the presence of condensed aromatics is also higher. Therefore, this coke has a more aromatic and condensed character than the one deposited during the cracking of STPO, which is directly related to the aromatic content of the two feeds. Similarly, the higher rate of vibration of C–H bonds for the coke from the cracking of STPO indicates that it has a more aliphatic character. This result is in accordance with those reported for FTIR/MS-TPO in Fig. 7d. On the other hand, the higher I_D/I_G ratio for the coke deposited during the cracking of VGO indicates that the coke clusters have a larger size. It is noteworthy to mention that the coke deposited during the cracking of the mixture

has intermediate rates compared to those of the individual feeds, but these rates are closer to those corresponding to the coke formed during the cracking of the STPO, indicating a further development of the coke formation mechanism from the STPO when the mix is fed.

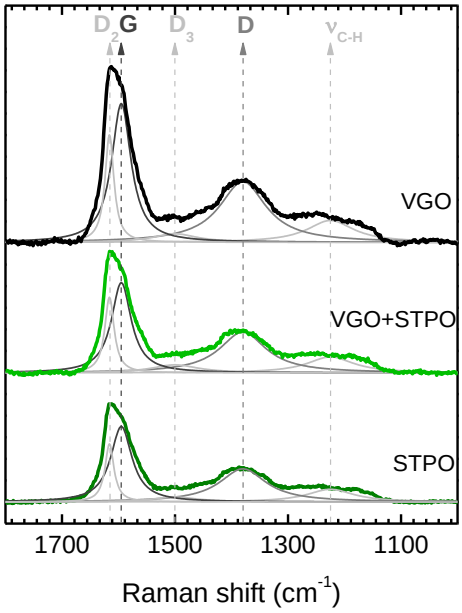

Fig. 8. Raman spectra of the coked catalyst for the different feeds used.

Table 3. Relative intensity (I) of the characteristic Raman spectra of the coked catalysts used with the different feeds.

	VGO	VGO+STPO	STPO
I_{C-H}	0.12	0.13	0.13
I_D	0.35	0.29	0.27
I_{D3}	0.06	0.05	0.05
I_G	0.35	0.32	0.30
I_{D2}	0.13	0.12	0.11
I_D/I_G	1.00	0.91	0.90

Laser desorption/ionization (LDI) time of flight (TOF) mass spectrometry has been used to characterize the aromatic components in the coke deposited on the catalyst used during the cracking of the three feeds (Fig. 9). These results show the nature of the coke deposited on the external surface of the catalyst particle, thus providing partial information that does not correspond to the coke deposited inside the pores of the zeolite or the matrix. Fig. 9 shows a notable difference between the spectra for the coked catalyst in the cracking of STPO and those corresponding to the other feeds. In the latter (with the VGO feed), majority species are identified in three fractions (100-190, 290-500 and 590-700 Da), while in the cracking of STPO only the two lightest fractions are formed. Furthermore, it is observed in the three catalysts that the difference between some adjacent peaks is 1 Da, which indicates the heterogeneous character of coke [57,70,76]. The masses with the highest intensity signals likely correspond to the compounds listed in Table 4, together with their molecular formula, the H/C ratio, and their possible structure. It is relevant that some of these compounds are not only common to the three feeds studied here, but also coincide with those observed by Cerqueira et al. [57] in the coke formed during the cracking of waste in a commercial FCC unit and by Ibarra et al. [70] in the coke formed during the cracking of diesel and bio-oil under FCC conditions.

The coke species in the range 290-500 Da can be ascribed to structures such as coronene ($C_{24}H_{12}$). The coke deposited during the cracking of VGO contains various species assigned to alkyl-coronenes (328, 342, and 356 Da) and alkyl-trybenzocoronenes (429 and 457 Da). These species can condensate further into benzodicoronene (596 Da) and its alkyl-benzodicoronene derivatives (662 and 668 Da). On the other hand, the tribenzocoronene condensates even further into hexabenzocoronene ($C_{48}H_{24}$) and its corresponding alkyl-hexabenzocoronene (628 Da). In regards to the spectrum of species detected in the cracking of STPO, the presence of the heaviest

coke species detected in the cracking of VGO is almost negligible. Alkyl-coronenes (342 Da) are still present and the incorporation of ethyl groups into the structure of tribenzocoronene (457, 485, and 513 Da) is also observed. On the other hand, the evolution of the coke structures will sequentially lead to the increase and decrease of the H/C ratio, as a consequence of the branching and condensation stages, respectively (Table 4). Based on these results, it is shown that the coke formed in the cracking of VGO or of the VGO+STPO mixture has polycyclic aromatic structures of high molecular weight, partially present in the VGO of the feed. Nevertheless, these structures are presumably formed mainly by the condensation of the lighter polycyclic aromatics in the VGO. The formation of these high molecular weight structures is less prevalent in the coke formed in the cracking of STPO, given the lower presence of polycyclic aromatics in the feed.

The qualitative and GC-MS analysis of the coke that is soluble in CH_2Cl_2 (external soluble coke) and of the one dissolved in CH_2Cl_2 once the zeolite crystal structure was destroyed by the HF treatment (internal soluble coke) are shown in Fig. 10 and Table 5. The soluble coke is mainly composed of light aromatics, with molecular weights in the range of 100-250 g mol^{-1}. Some of the components identified by GC-MS (Fig. 10) coincide with the lightest masses identified in the LDI-MS spectra of insoluble coke (Fig. 9), such as xylenes (106 g mol^{-1}) or tetralin (132 g mol^{-1}), indicating that these light compounds will be partially trapped in the polyaromatic structures.

Table 4. Most intense coke structures of the used catalysts in the LDI MS-TOF spectra.

Mass (Da)	Formula	H/C	Structure
106	C_8H_{10}	1.25	
132	$C_{10}H_{12}$	1.20	
328	$C_{26}H_{16}$	0.62	
342	$C_{27}H_{18}$	0.67	
356	$C_{28}H_{20}$	0.71	
429	$C_{33}H_{33}$	1.00	
457	$C_{35}H_{37}$	1.06	
487	$C_{37}H_{41}$	1.11	
513	$C_{39}H_{45}$	1.15	
596	$C_{48}H_{20}$	0.42	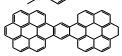
628	$C_{50}H_{28}$	0.56	
662	$C_{53}H_{26}$	0.49	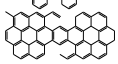
678	$C_{54}H_{30}$	0.56	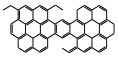

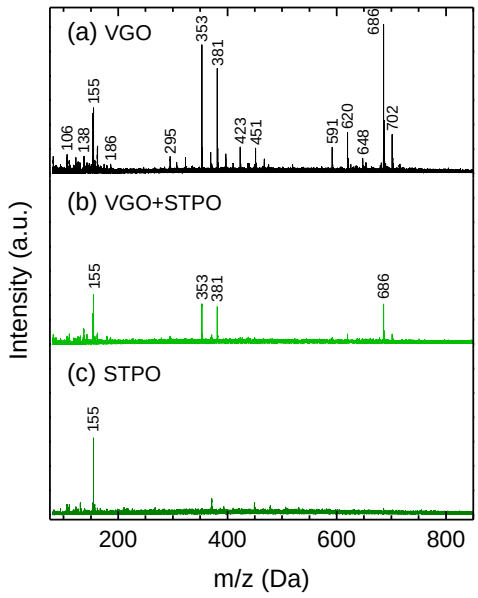

Fig. 9. LDI TOF-MS spectra of the used catalyst for the different feeds used.

Table 5 also depicts the results of the coke fractions determined following the coke extraction procedures. The coke deposited in the cracking of the VGO is mostly insoluble and the fraction of soluble coke is only 10%, which is in accordance with the condensed coke character determined from the TPO results. Furthermore, soluble coke is preferably deposited on the matrix and only a small fraction of the coke (around 1%) can be associated with the internal blockage of the micropores of the zeolite. Consequently, the deactivation of the catalyst in the cracking of the VGO can be attributed to the blocking of the mouths of the zeolite channels and not to the internal blocking of these channels.

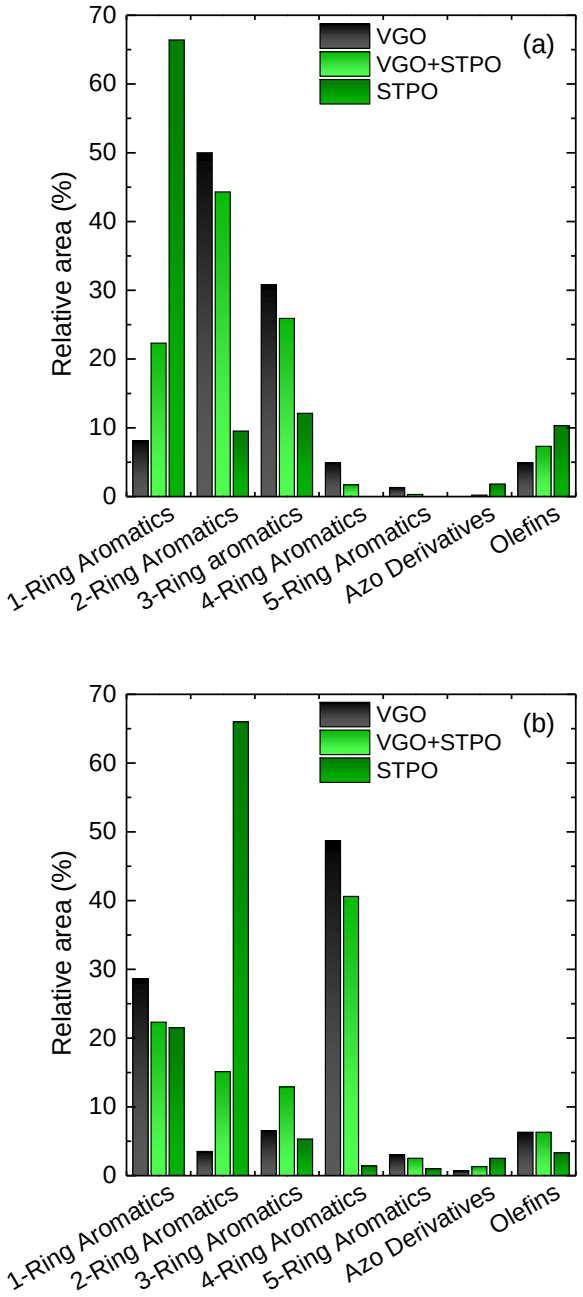

Fig. 10. GC-MS results of the dissolved cokes. (a) external coke. (b) internal coke.

Table 5. Coke fraction contents (wt%) deposited on the catalyst in the cracking of the three feeds.

	VGO	STPO + VGO	STPO
Total	1.55	1.32	1.02
Insoluble	1.39	1.03	0.57
Soluble	0.16	0.29	0.45
External	0.14	0.19	0.32
Internal	0.02	0.10	0.13

The coke formed from the STPO is remarkably different, with a higher fraction of soluble coke (44%) deposited on the outside (31% of the total) and inside (13% of the total) of the zeolite crystals. This difference with the coke deposited during the cracking of the VGO shows that the content of polycyclic aromatics in the feed has a strong incidence in the deposition of coke and that the high content of insoluble coke in the cracking of the VGO corresponds to polycyclic aromatics deposited on the matrix. This result is also consistent with the less condensed character of the coke from the cracking of STPO observed in the TPO results and with the limited incidence of deposition of polycyclic aromatics measured for the properties of micropores. Although these polycyclic aromatics will actually block hydrocarbon access to the micropores of the reaction medium, this partial blocking will not be sufficient to prevent N_2 diffusion in the adsorption-desorption analysis (Fig. 4); thus, being in accordance with the aforementioned result. On the other hand, the lower deposition of coke in the cracking of the STPO and its nature, with a lower external blocking capacity of the micropores, justifies the greater conversion obtained of this feed, evidenced by a higher gasoline yield compared to the one obtained in the cracking of VGO (Fig. 3). The lower external blockage of the micropores also justifies the greater effective

activity of the acid sites of the zeolite to take part in condensation reactions of coke precursor intermediates, with the formation of internal soluble coke.

In the cracking of the STPO+VGO mixture, the coke content is intermediate (1.32 wt%), with a lower value than that which would correspond to the independent cracking of each component of the mixture (1.44 wt%), which indicates a synergy in the coke deposition mechanism from the components of the mixture. The soluble coke content is intermediate (0.29 wt%) as well and higher than expected (0.22 wt%), also being notably higher the fraction of this soluble coke that is present inside the zeolite crystals. The effect of the composition of the feed on the deposition and nature of coke is well-established in the literature [54]. Moreover, the lower concentration of aromatic components that the VGO+STPO mixture contains compared to the VGO alone, and the greater adsorption capacity of these lighter reactants, both in the acid sites of the matrix and outside the zeolite crystals, may explain the aforementioned synergistic effect related to the content of coke. The adsorption of these lighter hydrocarbons presumably will hinder the adsorption of the polycyclic aromatics, and in general the condensation on the acid sites of the adsorbed coke structures. Furthermore, it is noteworthy to mention that this synergistic effect on the content and nature of coke has an impact on the synergy observed in the distribution of products. Thus, it is observed that the lower deposition of coke in the catalyst matrix (insoluble coke) has the consequence that the remaining activity for cracking of the HCO fraction is greater than expected, with a higher yield of the LCO and gasoline fraction products. On the other hand, the higher content of internal soluble coke (in the micropores of the zeolite) in the cracking of the mixture with respect to that theoretically expected, is consistent with the lower cracking capacity of gasoline to form LPG, a reaction that takes place on the active sites of the zeolite, which are directly blocked by light coke.

The lower deactivation of the catalyst with the STPO feed would justify the higher concentration of bicyclic aromatics, presumably located inside the channels and the formation of which from olefins is favored by the greater remaining capacity of the zeolite. However, the majority of the aromatic components in the internal coke of the VGO are of a tetracyclic aromatic nature, which can be formed in the zeolite supercages. Also, the lower olefin content in the internal coke of the cracking of STPO is consistent with the higher remaining activity of the catalyst for the condensation of olefins. The aromatic and olefin contents of the internal coke from the cracking of the mixture are equal to those of the coke obtained in the cracking of VGO, and the aromatic composition is intermediate to that of the cracking of the individual feeds. On the other hand, the presence of nitrogenous aromatics (azo derivatives) in the coke is significant in all cases except in external soluble coke from the cracking of VGO, which was also determined previously [57,70].

In addition, when the olefinic nature of the coke formed in the cracking of the three feeds that is soluble in CH_2Cl_2 is compared, it is observed that its concentration is higher outside the crystals than inside in all three cases. Additionally, the external soluble coke from STPO is more olefinic than that obtained from the cracking of VGO and that of the mixture. It should also be taking into account that olefinic hydrocarbons, like aromatic hydrocarbons, are considered precursors to coke [66] and that, of the studied feeds, STPO has the highest concentration of olefins in its composition.

4. Discussion

The results of the previous sections show, first of all, the difficulty in interpreting the results of the analysis of coke, since its nature is mainly conditioned by the severity of the reaction conditions in the FCC, especially by high reaction temperatures, as well as for the absence of

hydrogen in the reaction medium, which are conditions that favor the condensation of the coke components (aging) towards polycyclic aromatic structures. Furthermore, the feeds studied (VGO and STPO) have a high content of aromatics and olefins (in the case of STPO), with a high capacity to form a highly condensed coke on an acid catalyst. In terms of activity, this rapid deposition of the coke deactivates the catalyst in a few seconds, and the incidence of the composition of the feed, even if it is influenced by the reaction conditions, cannot be expected to be very relevant. However, the importance of the composition of the feed in the deposition, nature, and location of the coke is such that, through a combination of analytical techniques, significant differences in these phenomena were unveiled. The coke formed in the cracking of VGO has been found to be more condensed, which is consistent with the high content of polycyclic aromatics in this feed. These polycyclic aromatics are refractory to cracking and are partially retained in the macropores and mesopores of the catalyst matrix, which causes a decrease in the surface properties of the porous structure, attenuated by the generation of mesopores as spaces between the coke particles. The coke undergoes gradual condensation with the reaction time and is mostly insoluble in CH_2Cl_2 (Table 5). In regards to industrial operations, this coke corresponds to the name of Conradson Carbon (CCR) and, given the function of the matrix of the “filter” catalysts of these components, its deposition takes place preferably at the base of the riser reactor [53]. Given the steric hindrance of the access and diffusion of large polycyclic aromatics in the crystalline structure of the zeolite HY (openings of 7.4 Å with soldalite cages of 6.6 Å and supercages of 12.4 Å), the deactivation will take place by blocking the mouths of these micropores, preventing access of the hydrocarbons in the reaction medium (except aliphatic light components that are over-cracked with the formation of LPG, as well as with the undesired formation of dry gases) to the acid sites.

The hierarchization role of the porous structure of the FCC catalyst must be highlighted, where the zeolite matrix retains polycyclic aromatic coke, which is mostly insoluble in CH_2Cl_2, helping to attenuate the external blocking of micropores and therefore, the deactivation of the catalyst. Given the size of the pore openings of the zeolite HY, structures with a maximum of two aromatic rings could only be deposited inside the zeolite channels, which correspond to the majority of compounds present in the coke that is soluble in CH_2Cl_2 [77], as it is observed in Fig. 10. That being said, the inner cavities of the zeolite HY structure, also called supercages, may explain the presence of heavier aromatic components (made up of 3 and 4 rings) observed in the internal coke [78,79] of the coked catalysts used in the cracking of VGO and its mixture with STPO (Fig. 10b). Wang et al. [80] have demonstrated the growth of coke with greater aromatic condensation than the one allowed by the steric hindrance of the cages in the SAPO-34 catalyst during the methanol-to-olefins process. However, the heavier type of feed used here, the different zeolite used, the fact that the FCC catalyst contains matrix material, which can host coke molecules too, and the results presented in Fig. 4, point to the fact that the soluble coke analyzed in Table 5 corresponds to the one located within the micropores of the catalyst. Regarding soluble coke, a majority fraction will correspond to that deposited inside the zeolite crystals. This internal coke will presumably have a catalytic origin, being formed from the reactants by two routes; i) aromatic condensation and; ii) cyclization of olefins, dehydrogenation, and condensation [78]. An important role should also be expected from the acid sites on the external surface of the zeolite crystals, which are expected to partially maintain their activity (cracking and condensation of coke molecules) even if the micropores of the zeolite are blocked.

In the case of STPO, despite having a composition quite refractory to cracking, also has a notable olefin content and a lower aromatic content than VGO, the latter being mostly lighter as well

(one and two rings). These major components of STPO are also potential precursors to the formation of polycyclic aromatics [66]. In fact, the LDI-MS spectroscopy of insoluble coke has revealed that each of the samples have significantly different ranges and molecular weight distributions, but with matching growth sequences (Fig. 9). Consequently, in the reaction time used in this work (6 s), the coke deposited on the macro- and mesopores of the matrix, and on the outside of the zeolite crystals, is less developed than in the cracking of VGO. Considering the distribution of the products, it is observed that in the cracking of STPO, the blocking of the micropores of the zeolite takes place more slowly, and therefore, the remaining activity of the catalyst is greater for cracking the heavy fractions of the feed.

The content and nature of the coke formed in the cracking of the STPO + VGO mixture are a consequence of the different concentration (dilution) of the components with respect to the cracking of the two feeds individually, as well as to the synergy between the coke formation mechanisms. Hence, the concentration of aromatics is lower in the reaction medium, this factor attenuates the rate of condensation of the polycyclic aromatics, which in turn delays the blocking of the acidic sites of the matrix and the mouths of the micropores of the zeolite. These effects, verified when determining the contents of external and internal coke, will presumably prolong the activity of the acid sites in the matrix and inside these micropores, giving rise to the different distribution of products observed, with an improvement in the production of gasoline due to the cracking of the heavy components of the mixture.

Although the effect of STPO on the distribution of products is significant due to the aforementioned synergy on coke deposition, these differences in coke would not have a relevant importance in the operation of the regenerator of the FCC unit and in the unit energy balance. First, the FCC unit has the versatility necessary to operate stably with changes in feed

composition, and in particular for co-feeding other refinery streams. Furthermore, these other streams (such as distillation residues) are generally heavier, and generate higher amounts of polycyclic aromatic coke, suggesting that the incorporation of STPO would favor the co-feeding of residues or other highly aromatic streams. On the other hand, the sweeping with water vapor (in the "stripping" section) prior to the regenerator, will presumably be effective in the "aging" of the coke, making its composition (and later on its combustion) hardly differ from the usual, mitigating the impact of the power change on the operation of the regenerator and on the energy balance of the FCC unit.

In contrast, the LDI-MS analysis results of insoluble coke obtained after the destruction of the zeolite and the matrix structure with HF reveal that this fraction has significantly different ranges and molecular weight distributions in each of the samples (Fig. 9), but with matching growth sequences (Table 4). Therefore, it is assumed that the differences observed between the samples of the coked catalyst are mainly a consequence of the different nature of the feeds, and therefore, of the coke precursors. Consequently, the mechanism of coke formation in the catalyst used for the cracking of STPO and the STPO + VGO mixture under FCC conditions can be considered similar to that of VGO.

4. Conclusions

In this work we have proved the benefits of using scrap tire pyrolysis oil (STPO) as feed or co-feed in the fluid catalytic cracking unit. We have compared the cracking results of a benchmark feed (vacuum gas oil, VGO) in standard refinery unit conditions using a riser simulator. The products as well as the coked catalyst have been analyzed in detail using an arsenal of techniques.

Our results demonstrate that the cracking of STPO produces more gasoline, less light gases, less heavy gas-oils, and less coke. Not only has the cracking of STPO alone shown improvements in these parameters, but its partial addition to the regular FCC feedstock as VGO has also shown positive synergistic effects on the yields obtained.

We have delved into the effect that the addition of STPO has on lowering the deactivation of the catalyst. We have analyzed the deactivating deposits (coke) on the catalyst by characterizing it with several techniques. The coke deposited during the cracking of STPO is substantially more aliphatic, lighter, and is mainly located in the micropores of the catalyst. This result is linked to the average lighter nature of STPO as compared to the VGO.

The direct analysis of the coke and its different fractions have revealed the chemistry involved in its formation. Soluble coke species are mainly formed by one or two ring aromatic components, with a higher fraction of them located inside the pores when compared to insoluble coke species. Moreover, the presence of a higher fraction of this type of coke is related to higher conversions and lower average boiling point of feedstock. Insoluble coke species are mainly composed of polycyclic aromatic components, located in the matrix of the catalyst and outside the pores of the zeolite. They are responsible for the blocking of the zeolite pore mouths, which generates lower conversion levels and lower yields of desired product fractions like gasoline.

The results presented here allow us to positively frame the use of scrap tires in the refinery, not only from the point of view of valorization, but also to enhance the performance of the industrial units as the fluid catalytic cracking unit.

Conflict of interest

The authors declare no conflict of interests.

Acknowledgements

This research was funded by the Ministry of Economy and Competitiveness (MINECO) of the Spanish Government (CTQ2016-79646-P); the Ministry of Science, Innovation and Universities (MICINN) of the Spanish Governement (RTI2018-096981-B-100); the European Regional Development Funds (ERDF) and the Basque Government (IT1218-19). Dr. Rodriguez is thankful to the University of the Basque Country UPV/EHU (Zabalduz Programme). S. Izaddoust is thankful to the MINECO for her grant BES-2017-080077.

References

[1] Czajczyńska D, Krzyżyńska R, Jouhara H, Spencer N. Use of pyrolytic gas from waste tire as a fuel: A review. Energy 2017;134:1121–31. https://doi.org/10.1016/j.energy.2017.05.042.

[2] Güngör O, Tozlu A, Arslantürk C. A General Overview on Current status of ELT Management 3 rd International Conference on Advanced Engineering Technologies A General Overview on Current status of ELT Management 2019.

[3] Scott E. End-of-life Tyre Report. 2015.

[4] Torretta V, Rada EC, Ragazzi M, Trulli E, Istrate IA, Cioca LI. Treatment and disposal of tyres: Two EU approaches. A review. Waste Manag 2015;45:152–60. https://doi.org/10.1016/j.wasman.2015.04.018.

[5] Hita I, Arabiourrutia M, Olazar M, Bilbao J, Arandes JM, Castaño Sánchez P. Opportunities and barriers for producing high quality fuels from the pyrolysis of scrap tires. Renew Sustain Energy Rev 2016;56:745–59.

https://doi.org/10.1016/j.rser.2015.11.081.

[6] Rowhani A, Rainey TJ. Scrap tyre management pathways and their use as a fuel - A review. Energies 2016;9:1–26. https://doi.org/10.3390/en9110888.

[7] Muelas Á, Callén MS, Murillo R, Ballester J. Production and droplet combustion characteristics of waste tire pyrolysis oil. Fuel Process Technol 2019;196:106149. https://doi.org/10.1016/j.fuproc.2019.106149.

[8] Halle LL, Palmqvist A, Kampmann K, Khan FR. Ecotoxicology of micronized tire rubber: Past, present and future considerations. Sci Total Environ 2020;706:135694. https://doi.org/10.1016/j.scitotenv.2019.135694.

[9] Jan Kole P, Löhr AJ, Van Belleghem FGAJ, Ragas AMJ. Wear and tear of tyres: A stealthy source of microplastics in the environment. Int J Environ Res Public Health 2017;14. https://doi.org/10.3390/ijerph14101265.

[10] Fauser P, Tjell JC, Mosbaek H, Pilegaard K. Tire-tread and bitumen particle concentrations in aerosol and soil samples. Pet Sci Technol 2002;20:127–41. https://doi.org/10.1081/LFT-120002092.

[11] Zang G, Jia J, Shi Y, Sharma T, Ratner A. Modeling and economic analysis of waste tire gasification in fluidized and fixed bed gasifiers. Waste Manag 2019;89:201–11. https://doi.org/https://doi.org/10.1016/j.wasman.2019.03.070.

[12] Machin EB, Pedroso DT, de Carvalho JA. Technical assessment of discarded tires gasification as alternative technology for electricity generation. Waste Manag 2017;68:412–20. https://doi.org/https://doi.org/10.1016/j.wasman.2017.07.004.

[13] Elbaba IF, Williams PT. Two stage pyrolysis-catalytic gasification of waste tyres:

Influence of process parameters. Appl Catal B Environ 2012;125:136–43. https://doi.org/10.1016/j.apcatb.2012.05.020.

[14] Toledo M, Ripoll N, Céspedes J, Zbogar-Rasic A, Fedorova N, Jovicic V, et al. Syngas production from waste tires using a hybrid filtration reactor under different gasifier agents. Energy Convers Manag 2018;172:381–90. https://doi.org/10.1016/j.enconman.2018.07.046.

[15] Hervy M, Remy D, Dufour A, Mauviel G. Air-blown gasification of Solid Recovered Fuels (SRFs) in lab-scale bubbling fluidized-bed: Influence of the operating conditions and of the SRF composition. Energy Convers Manag 2019;181:584–92. https://doi.org/10.1016/j.enconman.2018.12.052.

[16] Hoang AT, Nguyen TH, Nguyen HP. Scrap tire pyrolysis as a potential strategy for waste management pathway: a review. Energy Sources, Part A Recover Util Environ Eff 2020:1–18. https://doi.org/10.1080/15567036.2020.1745336.

[17] Hu Q, Tang Z, Yao D, Yang H, Shao J, Chen H. Thermal behavior, kinetics and gas evolution characteristics for the co-pyrolysis of real-world plastic and tyre wastes. J Clean Prod 2020;260:121102. https://doi.org/https://doi.org/10.1016/j.jclepro.2020.121102.

[18] Wang J, Zhong Z, Ding K, Li M, Hao N, Meng X, et al. Catalytic fast co-pyrolysis of bamboo sawdust and waste tire using a tandem reactor with cascade bubbling fluidized bed and fixed bed system. Energy Convers Manag 2019;180:60–71. https://doi.org/10.1016/j.enconman.2018.10.056.

[19] Xu F, Wang B, Yang D, Ming X, Jiang Y, Hao J, et al. TG-FTIR and Py-GC/MS study on pyrolysis mechanism and products distribution of waste bicycle tire. Energy Convers

Manag 2018;175:288–97. https://doi.org/10.1016/j.enconman.2018.09.013.

[20] Lewandowski WM, Januszewicz K, Kosakowski W. Efficiency and proportions of waste tyre pyrolysis products depending on the reactor type—A review. J Anal Appl Pyrolysis 2019;140:25–53. https://doi.org/10.1016/j.jaap.2019.03.018.

[21] Arabiourrutia M, Lopez G, Elordi G, Olazar M, Aguado R, Bilbao J. Product distribution obtained in the pyrolysis of tyres in a conical spouted bed reactor. Chem Eng Sci 2007;62:5271–5. https://doi.org/10.1016/j.ces.2006.12.026.

[22] Troca-Torrado C, Alexandre-Franco M, Fernández-González C, Alfaro-Domínguez M, Gómez-Serrano V. Development of adsorbents from used tire rubber: Their use in the adsorption of organic and inorganic solutes in aqueous solution. Fuel Process Technol 2011;92:206–12. https://doi.org/10.1016/j.fuproc.2010.03.007.

[23] Koc AB, Abdullah M. Performance of a 4-cylinder diesel engine running on tire oil-biodiesel-diesel blend. Fuel Process Technol 2014;118:264–9. https://doi.org/10.1016/j.fuproc.2013.09.013.

[24] Frigo S, Seggiani M, Puccini M, Vitolo S. Liquid fuel production from waste tyre pyrolysis and its utilisation in a Diesel engine. Fuel 2014;116:399–408. https://doi.org/10.1016/j.fuel.2013.08.044.

[25] Williams PT. Pyrolysis of waste tyres: A review. Waste Manag 2013;33:1714–28. https://doi.org/https://doi.org/10.1016/j.wasman.2013.05.003.

[26] Lopez G, Alvarez J, Amutio M, Mkhize NM, Danon B, van der Gryp P, et al. Waste truck-tyre processing by flash pyrolysis in a conical spouted bed reactor. Energy Convers Manag 2017;142:523–32. https://doi.org/https://doi.org/10.1016/j.enconman.2017.03.051.

[27] Wang J, Jiang J, Wang X, Liu P, Li J, Liu G, et al. Catalytic conversion of rubber wastes to produce aromatic hydrocarbons over USY zeolites: Effect of SiO2/Al2O3 mole ratio. Energy Convers Manag 2019;197. https://doi.org/10.1016/j.enconman.2019.111857.

[28] Januszewicz K, Kazimierski P, Kosakowski W, Lewandowski WM. Waste Tyres Pyrolysis for Obtaining Limonene. Materials (Basel) 2020;13:1359. https://doi.org/10.3390/ma13061359.

[29] Rodríguez E, Gutiérrez A, Palos R, Azkoiti MJ, Arandes JM, Bilbao J. Cracking of Scrap Tires Pyrolysis Oil in a Fluidized Bed Reactor under Catalytic Cracking Unit Conditions. Effects of Operating Conditions. Energy and Fuels 2019;33:3133–43. https://doi.org/10.1021/acs.energyfuels.9b00292.

[30] Rodríguez E, Palos R, Gutiérrez A, Arandes JM, Bilbao J. Production of Non-Conventional Fuels by Catalytic Cracking of Scrap Tires Pyrolysis Oil. Ind Eng Chem Res 2019. https://doi.org/10.1021/acs.iecr.9b00632.

[31] Bai P, Etim UJ, Yan Z, Mintova S, Zhang Z, Zhong Z, et al. Fluid catalytic cracking technology: current status and recent discoveries on catalyst contamination. Catal Rev - Sci Eng 2019;61:333–405. https://doi.org/10.1080/01614940.2018.1549011.

[32] Alvira J, Hita I, Rodríguez E, Arandes J, Castaño P. A Data-Driven Reaction Network for the Fluid Catalytic Cracking of Waste Feeds. Processes 2018;6:243. https://doi.org/10.3390/pr6120243.

[33] Dupain X, Krul RA, Schaverien CJ, Makkee M, Moulijn JA. Production of clean transportation fuels and lower olefins from Fischer-Tropsch Synthesis waxes under fluid catalytic cracking conditions: The potential of highly paraffinic feedstocks for FCC. Appl

Catal B Environ 2006;63:277–95. https://doi.org/10.1016/j.apcatb.2005.10.012.

[34] García JR, Falco M, Sedran U. Intracrystalline mesoporosity over Y zeolites. Processing of VGO and resid-VGO mixtures in FCC. Catal Today 2017;296:247–53. https://doi.org/10.1016/j.cattod.2017.04.010.

[35] Arandes JM, Azkoiti MJ, Torre I, Olazar M, Castaño P. Effect of HZSM-5 catalyst addition on the cracking of polyolefin pyrolysis waxes under FCC conditions. Chem Eng J 2007;132:17–26. https://doi.org/10.1016/j.cej.2007.01.012.

[36] Corma A, Sauvanaud L. FCC testing at bench scale: New units, new processes, new feeds. Catal Today 2013;218–219:107–14. https://doi.org/10.1016/j.cattod.2013.03.038.

[37] Vogt ETC, Weckhuysen BM. Fluid catalytic cracking: recent developments on the grand old lady of zeolite catalysis. Chem Soc Rev 2015;44:7342–70. https://doi.org/10.1039/c5cs00376h.

[38] Gerards RTJ, Fernandes A, Graça I, Ribeiro MF. Towards understanding of phenolic compounds impact on Ni- and V-USY zeolites during bio-oils co-processing in FCC units. Fuel 2020;260:116372. https://doi.org/10.1016/j.fuel.2019.116372.

[39] Talmadge MS, Baldwin RM, Biddy MJ, McCormick RL, Beckham GT, Ferguson GA, et al. A perspective on oxygenated species in the refinery integration of pyrolysis oil. Green Chem 2014;16:407–53. https://doi.org/10.1039/c3gc41951g.

[40] Manara P, Bezergianni S, Pfisterer U. Study on phase behavior and properties of binary blends of bio-oil/fossil-based refinery intermediates: A step toward bio-oil refinery integration. Energy Convers Manag 2018;165:304–15. https://doi.org/10.1016/j.enconman.2018.01.023.

[41] Behr A, Bayrak Z, Samli G, Yildiz D, Peitz S, Stochniol G. Oligomerization of n-Butenes in a Two-Phase Reaction System with Homogeneous Ni/Al-Catalysts. Chem Eng Technol 2016;39:263–70. https://doi.org/10.1002/ceat.201500317.

[42] Stefanidis SD, Kalogiannis KG, Lappas AA. Co-processing bio-oil in the refinery for drop-in biofuels via fluid catalytic cracking. Wiley Interdiscip Rev Energy Environ 2018;7. https://doi.org/10.1002/wene.281.

[43] Ibarra A, Rodríguez E, Sedran U, Arandes JM, Bilbao J. Synergy in the Cracking of a Blend of Bio-oil and Vacuum Gasoil under Fluid Catalytic Cracking Conditions. Ind Eng Chem Res 2016;55:1872–80. https://doi.org/10.1021/acs.iecr.5b04502.

[44] Pujro R, Panero M, Bertero M, Sedran U, Falco M. Hydrogen Transfer between Hydrocarbons and Oxygenated Compounds in Coprocessing Bio-Oils in Fluid Catalytic Cracking. Energy & Fuels 2019;33:6473–82. https://doi.org/10.1021/acs.energyfuels.9b01133.

[45] Bertero M, Puente GDL, Sedran U. Products and coke from the conversion of bio-oil acids, esters, aldehydes and ketones over equilibrium FCC catalysts. Renew Energy 2013;60:349–54. https://doi.org/10.1016/j.renene.2013.04.017.

[46] Santillan-Jimenez E, Pace R, Morgan T, Behnke C, Sajkowski DJ, Lappas A, et al. Co-processing of hydrothermal liquefaction algal bio-oil and petroleum feedstock to fuel-like hydrocarbons via fluid catalytic cracking. Fuel Process Technol 2019. https://doi.org/10.1016/j.fuproc.2019.02.018.

[47] Sanahuja-Parejo O, Veses A, Navarro M V., López JM, Murillo R, Callén MS, et al. Catalytic co-pyrolysis of grape seeds and waste tyres for the production of drop-in

biofuels. Energy Convers Manag 2018;171:1202–12. https://doi.org/10.1016/j.enconman.2018.06.053.

[48] Passamonti FJ, Sedran U. Recycling of waste plastics into fuels. LDPE conversion in FCC. Appl Catal B Environ 2012;125:499–506. https://doi.org/10.1016/j.apcatb.2012.06.020.

[49] Rodríguez E, Gutiérrez A, Palos R, Vela FJ, Azkoiti MJ, Arandes JM, et al. Co-cracking of high-density polyethylene (HDPE) and vacuum gasoil (VGO) under refinery conditions. Chem Eng J 2020;382. https://doi.org/10.1016/j.cej.2019.122602.

[50] Wang C, Tian X, Zhao B, Zhu L, Li S. Experimental Study on Spent FCC Catalysts for the Catalytic Cracking Process of Waste Tires. Processes 2019;7:335. https://doi.org/10.3390/pr7060335.

[51] Rodríguez E, Palos R, Gutiérrez A, Arandes JM, Bilbao J. Scrap tires pyrolysis oil as a co-feeding stream on the catalytic cracking of vacuum gasoil under fluid catalytic cracking conditions. Waste Manag 2020;105:18–26. https://doi.org/10.1016/j.wasman.2020.01.026.

[52] Rodríguez E, Elordi G, Valecillos J, Izaddoust S, Bilbao J, Arandes JM, et al. Coke deposition and product distribution in the co-cracking of waste polyolefin derived streams and vacuum gas oil under FCC unit conditions. Fuel Process Technol 2019;192:130–9. https://doi.org/10.1016/j.fuproc.2019.04.012.

[53] Fernandes JL, Domingues LH, Pinheiro CIC, Oliveira NMC, Ribeiro FR. Influence of different catalyst deactivation models in a validated simulator of an industrial UOP FCC unit with high-efficiency regenerator. Fuel 2012;97:97–108. https://doi.org/10.1016/j.fuel.2012.03.009.

[54] Cerqueira HS, Caeiro G, Costa L, Ramôa Ribeiro F. Deactivation of FCC catalysts. J Mol Catal A Chem 2008;292:1–13. https://doi.org/10.1016/j.molcata.2008.06.014.

[55] Almas Q, Naeem MA, Baldanza MAS, Solomon J, Kenvin JC, Müller CR, et al. Transformations of FCC catalysts and carbonaceous deposits during repeated reaction-regeneration cycles. Catal Sci Technol 2019;9:6977–92. https://doi.org/10.1039/c9cy01680e.

[56] Etim UJ, Wu P, Bai P, Xing W, Ullah R, Subhan F, et al. Location and Surface Species of Fluid Catalytic Cracking Catalyst Contaminants: Implications for Alleviating Catalyst Deactivation. Energy & Fuels 2016;30:10371–82. https://doi.org/10.1021/acs.energyfuels.6b02505.

[57] Cerqueira HS, Sievers C, Joly G, Magnoux P, Lercher JA. Multitechnique characterization of coke produced during commercial resid FCC operation. Ind Eng Chem Res 2005;44:2069–77. https://doi.org/10.1021/ie048963k.

[58] Zhang YS, Lu X, Owen RE, Manos G, Xu R, Wang FR, et al. Fine structural changes of fluid catalytic catalysts and characterization of coke formed resulting from heavy oil devolatilization. Appl Catal B Environ 2020;263. https://doi.org/10.1016/j.apcatb.2019.118329.

[59] Meirer F, Kalirai S, Morris D, Soparawalla S, Liu Y, Mesu G, et al. Life and death of a single catalytic cracking particle. Sci Adv 2015;1:1–13. https://doi.org/10.1126/sciadv.1400199.

[60] Gambino M, Veselý M, Filez M, Oord R, Ferreira Sanchez D, Grolimund D, et al. Nickel Poisoning of a Cracking Catalyst Unravelled by Single-Particle X-ray Fluorescence-

Diffraction-Absorption Tomography. Angew Chemie - Int Ed 2020;59:3922–7. https://doi.org/10.1002/anie.201914950.

[61] Krumeich F, Ihli J, Shu Y, Cheng W-C, van Bokhoven JA. Structural Changes in Deactivated Fluid Catalytic Cracking Catalysts Determined by Electron Microscopy. ACS Catal 2018;8:4591–9. https://doi.org/10.1021/acscatal.8b00649.

[62] Ihli J, Jacob RR, Holler M, Guizar-Sicairos M, Diaz A, Da Silva JC, et al. A three-dimensional view of structural changes caused by deactivation of fluid catalytic cracking catalysts. Nat Commun 2017;8. https://doi.org/10.1038/s41467-017-00789-w.

[63] Lopez G, Alvarez J, Amutio M, Mkhize NM, Danon B, van der Gryp P, et al. Waste truck-tyre processing by flash pyrolysis in a conical spouted bed reactor. Energy Convers Manag 2017;142:523–32. https://doi.org/10.1016/j.enconman.2017.03.051.

[64] Alvarez J, Lopez G, Amutio M, Mkhize NM, Danon B, van der Gryp P, et al. Evaluation of the properties of tyre pyrolysis oils obtained in a conical spouted bed reactor. Energy 2017;128:463–74. https://doi.org/10.1016/j.energy.2017.03.163.

[65] Castaño P, Gutiérrez A, Villanueva I, Pawelec B, Bilbao J, Arandes JM. Effect of the support acidity on the aromatic ring-opening of pyrolysis gasoline over Pt/HZSM-5 catalysts. Catal Today 2009;143:115–9. https://doi.org/10.1016/j.cattod.2008.10.029.

[66] Bauer F, Karge HG. Characterization of coke on zeolites. Mol Sieves - Sci Technol 2006;5:249–364. https://doi.org/10.1007/3829_005.

[67] Palos R, Kekäläinen T, Duodu F, Gutiérrez A, Arandes JM, Jänis J, et al. Screening hydrotreating catalysts for the valorization of a light cycle oil/scrap tires oil blend based on a detailed product analysis. Appl Catal B Environ 2019.

https://doi.org/10.1016/j.apcatb.2019.117863.

[68] Aguayo AT, Castaño P, Mier D, Gayubo AG, Olazar M, Bilbao J. Effect of cofeeding butane with methanol on the deactivation by coke of a HZSM-5 zeolite catalyst. Ind Eng Chem Res 2011;50:9980–8. https://doi.org/10.1021/ie200946n.

[69] Castaño P, Elordi G, Olazar M, Aguayo AT, Pawelec B, Bilbao J. Insights into the coke deposited on HZSM-5, Hβ and HY zeolites during the cracking of polyethylene. Appl Catal B Environ 2011;104:91–100. https://doi.org/10.1016/j.apcatb.2011.02.024.

[70] Ibarra A, Veloso A, Bilbao J, Arandes JM, Castaño P. Dual coke deactivation pathways during the catalytic cracking of raw bio-oil and vacuum gasoil in FCC conditions. Appl Catal B Environ 2016;182:336–46. https://doi.org/10.1016/j.apcatb.2015.09.044.

[71] Aguayo AT, Gayubo AG, Ereña J, Atutxa A, Bilbao J. Coke Aging and Its Incidence on Catalyst Regeneration. Ind Eng Chem Res 2003;42:3914–21. https://doi.org/10.1021/ie030085n.

[72] Magnoux P, Cerqueira HS, Guisnet M. Evolution of coke composition during ageing under nitrogen. Appl Catal A Gen 2002;235:93–9. https://doi.org/10.1016/S0926-860X(02)00242-9.

[73] Epelde E, Ibañez M, Aguayo AT, Gayubo AG, Bilbao J, Castaño P. Differences among the deactivation pathway of HZSM-5 zeolite and SAPO-34 in the transformation of ethylene or 1-butene to propylene. Microporous Mesoporous Mater 2014;195:284–93. https://doi.org/10.1016/j.micromeso.2014.04.040.

[74] Guichard B, Roy-Auberger M, Devers E, Rebours B, Quoineaud AA, Digne M. Characterization of aged hydrotreating catalysts. Part I: Coke depositions, study on the

chemical nature and environment. Appl Catal A Gen 2009;367:1–8. https://doi.org/10.1016/j.apcata.2009.07.024.

[75] Roberston J. Diamond-like amorphous carbon. Mater Sci Eng R-Reports 2002;37:129. https://doi.org/10.1016/S0927-796X(02)00005-0.

[76] Cordero-Lanzac T, Hita I, Veloso A, Arandes JM, Rodríguez-Mirasol J, Bilbao J, et al. Characterization and controlled combustion of carbonaceous deactivating species deposited on an activated carbon-based catalyst. Chem Eng J 2017;327:454–64. https://doi.org/10.1016/j.cej.2017.06.077.

[77] Magnoux P, Roger P, Canaff C, Fouche V, Gnep NS, Guisnet M. New technique for the characterization of carbonaceous compounds responsible for zeolite deactivation. Stud. Surf. Sci. Catal., vol. 34, 1987, p. 317–30. https://doi.org/10.1016/S0167-2991(09)60370-0.

[78] Guisnet M, Magnoux P. Organic chemistry of coke formation. Appl Catal A Gen 2001. https://doi.org/10.1016/S0926-860X(00)00845-0.

[79] Elordi G, Olazar M, Lopez G, Castaño P, Bilbao J. Role of pore structure in the deactivation of zeolites (HZSM-5, Hβ and HY) by coke in the pyrolysis of polyethylene in a conical spouted bed reactor. Appl Catal B Environ 2011;102:224–31. https://doi.org/10.1016/j.apcatb.2010.12.002.

[80] Wang N, Zhi Y, Wei Y, Zhang W, Liu Z, Huang J, et al. Molecular elucidating of an unusual growth mechanism for polycyclic aromatic hydrocarbons in confined space. Nat Commun 2020;11. https://doi.org/10.1038/s41467-020-14493-9.